Infrared Physics & Technology 155 (2026) 106497

Contents lists available at ScienceDirect

Infrared Physics and Technology

journal homepage: www.elsevier.com/locate/infrared

Research Paper

Compact trace gas sensing via single-cavity balanced-detection interferometric cavity-assisted photothermal spectroscopy

Johannes P. Waclawek *, Harald Moser, Ufuk Yilmaz, Bernhard Lendl

TU Wien – Vienna University of Technology, Getreidemarkt 9/164-UPA, 1060 Wien, Austria

ARTICLE INFO

Keywords:
Interferometry
Fabry-Perot
Balanced detection
Laser sensors
Photothermal spectroscopy
Infrared spectroscopy

ABSTRACT

This work reports on the implementation of an alternative balanced-detection scheme to the ICAPS sensing method employing solely a single cavity. The new concept was realized by simultaneous detection of the interferometer's reflectance and transmission. The use of only one cavity significantly reduces the system's complexity in a balanced configuration by simplifying the detection architecture. Additionally, it increases the sensor's sensitivity by noise cancellation and an improvement of the detectable signal up to a factor of 2. The set-up employed an optical cavity with a mirror spacing of 1 mm. A mid-infrared laser served as excitation source to induce refractive index changes in the sample, and a near-infrared laser served as probe source to monitor the photo-induced variations. The sensor's metrological figures of merit were investigated by detection of CO. Moreover, the influence of varying water vapor concentration on the molecular relaxation of CO and thus the monitored photothermal signal employing a modulation frequency of ~ 300 Hz was investigated. For the targeted absorption band centered at 2179.77 cm^{-1} a 1σ minimum detection limit of 2 ppbv was achieved using an integration time of 1 s. This result corresponds to a normalized noise equivalent absorption of 7.4×10^{-9} cm^{-1} W $Hz^{-1/2}$.

1. Introduction

The miniaturization of sensitive as well as selective gas sensors is of high interest across a variety of application fields; however, achieving such a sensor platform remains a challenging task. Decreasing the sample gas volume required by the sensor may be beneficial for several reasons: It facilitates a quick gas exchange, thereby enabling the monitoring of rapid changes of analyte concentration levels in a sample stream. It may also be advantageous for use cases where the available sample volume is limited to a few mm^3 or even below. Moreover, a small sensor footprint is requested for development of mobile applications and is also advantageous for integration into existing settings such as of process analytical technology (PAT) applications, where only limited space is available and access to the process stream is difficult. Applications of laser-based gas sensors may be found in industry for process and product quality control, gas leak detection, environmental monitoring, medical studies, or scientific research [1–6]. Conventional sensing techniques based on direct absorption spectroscopy, i.e. methods which directly measure the attenuation of the light, have an inherently restricted potential for miniaturization due to the dependency of their sensitivity on the optical path length according to the Beer-Lambert law. Nevertheless, these well-established as well as recently developed systems show clear merits regarding robustness, multi-component analysis, calibration-free detection, fast data recording, implementation of modulation strategies and signal modeling [7–12]. In contrast, indirect absorption spectroscopy methods, i.e. methods which measure an effect that the absorption of light has on the sample including photothermal spectroscopy (PTS) and photoacoustic spectroscopy (PAS), offer great potential for sensor miniaturization. This is especially true for PTS employing a Fabry-Perot interferometer (FPI) as the transducer. Moreover, indirect absorption spectroscopy techniques show clear benefits of a decades-spanning dynamic range and background-free detection [13]. Also, multi-component detection employing PAS has been shown [14,15]. Photothermal gas spectroscopy methods typically use an excitation laser to induce a signal and a probe laser to monitor the magnitude of the generated signal: molecules absorbing the excitation source lead to a temperature change of the sample. This in turn leads to a pressure and density change, causing the generation of a pressure and thermal wave. The thermal wave causes a change in the refractive index of the sample which is monitored by the probe laser [16]. As the thermal

* Corresponding author.
E-mail address: johannes.waclawek@tuwien.ac.at (J.P. Waclawek).

https://doi.org/10.1016/j.infrared.2026.106497
Received 17 December 2025; Received in revised form 21 February 2026; Accepted 1 March 2026
Available online 4 March 2026

wave only expands in the very vicinity of its generation, PTS systems can be truly miniaturized, in principle even down to photonic integration on chip scale.

PTS has been carried out using different types of interferometers in different settings, ranging from simple free-spaced FPI configurations [17–22] to instruments employing a FPI inside hollow-core fibers FPI [23] or a Mach-Zehnder interferometer [24], or mode-phase-difference interferometry [25]. An all-fiber intra-cavity photothermal gas sensor based on a Sagnac interferometer [26] and an intra-cavity photothermal detection in a mode-locked laser configuration [27] have also been demonstrated. In the case of interferometric readout the system's responsivity is in general a function of the induced phase difference of the interfering probe laser waves inside the interferometer [16]. The variation in the phase difference is then transduced into a variation of the transmitted probe laser power. In case of a FPI, the phase difference is among other parameters dependent on the induced refractive index change and the mirror spacing. In addition, the sensitivity of such a sensor is dependent on the cavity finesse, which in turn is a function of the mirror reflectivity. The finesse allows compensation of a reduced phase difference emerging by a small interferometer path-length via employing moderate to high mirror reflectivity. Thereby, the FPI allows for construction of miniaturized but highly sensitive transducers. PTS employing a FPI for transducing photo-induced variations is a highly capable approach for gas detection. As such, the *Interferometric Cavity-Assisted Photothermal Spectroscopy* (ICAPS) technique [18–20] has been demonstrated to be a sensitive and compact realization of a PTS based gas sensor technology. It utilizes an air-spaced Fabry-Perot cavity having a short mirror gap together with a moderate finesse. Advanced designs of the ICAPS arrangement employing a reference path and balanced detection have shown detection limits in the low parts-per-billion by volume (ppbv) range with a corresponding normalized noise equivalent absorption (NNEA) in the order of 10^{-9} cm^{-1} W $Hz^{-1/2}$ [19,20]. Also, the arrangement of a fiber-array with attached micro-lenses to the balanced-detection ICAPS layout has been shown recently with two cavities probed in one interferometric device [28]. The balanced-detection ICAPS technique links the general advantage of using an optical cavity in photothermal spectroscopy together with the advantage of noise rejection down to the shot noise limit. So far, balanced detection ICAPS has only be shown using two cavities. In this work, we show for the first time an approach to balance the ICAPS signal employing only a single cavity, significantly reducing the complexity and operation of the detection scheme.

2. Basic ICAPS sensor operation, sources of noise and noise cancellation

2.1. Basic ICAPS sensor operation

The basic ICAPS configuration [18] consists of an air-spaced Fabry-Perot interferometer (FPI), a probe beam which is transmitted through the interferometer, a photodiode which is monitoring the transmitted probe laser power and an excitation beam which induces refractive index changes. The FPI, i.e., an optical cavity, comprises of two partially transmitting mirrors and the gaseous medium in between the mirrors. It is excellently suited to detect minute changes in the refractive index of a gaseous sample by monitoring the phase difference of the probe laser passing through it. Laser radiation entering the FPI will be partially reflected by the input mirror, whereas the transmitted part is reflected multiple times in between the two mirrors forming the optical cavity. In this manner an infinite series of partial waves in forward and backward direction is formed. Upon each reflection at both mirrors, laser radiation is coupled out from the cavity either in the forward or backward direction. The periodic resonances of an ideal FPI is described by the Airy function [29,30]. Its properties are dependent on the phase difference for a cavity round trip as well as on the cavity's finesse. The phase difference is a function of the vacuum wavelength, the angle of incidence, the spacing of the mirrors, and the refractive index of the medium between the mirrors. The finesse is defined by the mirrors reflectivity. The transmittance of the FPI is maximized at resonance, whereas its reflectance is minimized at this frequency. The beam which is transmitted through the interferometer is simply the part of the standing wave inside the cavity, leaking out at the second mirror. The reflected beam, however, is composed by the sum of two beams interfering with each other: the fraction which is immediately reflected at the input mirror as well as the fraction which is leaking out of the interferometer through this first mirror.

The ICAPS operation can be employed for both, the forward transmitted light [18,19] as well as for the backward reflected light [20,28]. In any case an excitation laser is used to heat a gas sample transiently within the FPI, thereby inducing a modulated change in the sample's refractive index. As the index of refraction of the gas alters due to analyte absorption, the periodic resonances of the interferometer are frequency shifted. This shift is monitored via the probe laser, which probes the interferometer's resonance in combination with a photodiode. The most sensitive region for transducing changes in the phase difference is located around the inflection points of the cavities' resonance. These points are at around 25 % of the top of the resonance in case of reflectance and at around 75 % of the top of the resonance in case of transmittance. Around the inflection point the functions' slope is largest and in first proximity linear within a small range, generating a linear transducer signal to refractive index variations.

2.2. Sources of noise and noise cancellation

The basic ICAPS sensing scheme [18] detects photo-induced refractive index changes but is susceptible to noise of different sources. The principal sources of noise are probe laser and environmental noise. The probe laser beam itself carries intensity as well as frequency noise. By tuning the probe laser frequency to an inflection point of the cavity resonance, the probe beam's intensity noise will pass through the cavity without any amplification of its amplitude, being unaffected by the shape of the cavity's resonance. However, the amplitude of the frequency noise contribution is amplified according to the steepness of the resonances slope. The characteristics of the probe lasers intensity and frequency noise are subject of the employed laser type [29] and of its operation. Different driving currents may yield different intensity fluctuations, or a noisy driving source may influence the laser's output quality. Additionally, noise from the surroundings may be coupled into the system by acoustic or mechanical impact. Acoustic waves modulate the sample's index of refraction as a result of pressure changes. These changes will cause shifts of the cavity resonances similar to photothermally generated refractive index alterations. Again, transduced signals of interfering acoustic waves will be directly amplified according to the utilized slope's steepness. Mechanical impacts may cause tiny changes in the interferometers geometry which may affect the transmission function's shape and position.

An effective way to reject noise in an ICAPS setup has been shown by the implementation of a balanced detection scheme [19,20]. In these setups common-mode noise is cancelled by concurrently detection of the probe lasers intensity with and without the photothermal contribution. For this purpose, the probe beam is divided in two alike parts, a sample probe beam and a reference probe beam. The two parts are subsequently transmitted into two interferometers, a sample cavity and a reference cavity. The sample probe beam crosses the excitation beam inside the cavity, passing through the transiently heated gas zone. This beam carries both, the transduced photothermal signal together with noise. The reference probe beam, however, solely carries noise as it does not pass through the generated photothermal waves. The two beams are detected by two separate photodiodes, whose outputs are electronically subtracted. This method has the clear benefit that it allows for elimination of the noise contributions which are equal in both branches with a high common-mode rejection ratio down to the sensors fundamental

limit of shot noise. This scheme increases the sensor's sensitivity by improving the signal-to-noise ratio but also the sensor's robustness by elimination of environmental noise such as sound. This very effective method, however, comes with the downside of increased system complexity. It requires the operation of two independent FPIs together with the corresponding sample and reference beams. A less complex, but still effective method for noise cancellation is proposed in this work. It can be realized by simultaneous detection of a single cavity's reflectance and transmittance.

3. Balanced-detection ICAPS employing a single cavity

The scheme of balanced-detection ICAPS employing a single cavity is depicted in Fig. 1. The setup uses an all fiber-coupled probe laser configuration. The probe beam is directly coupled into the interferometer where it intersects with the excitation beam. In presence of targeted analyte molecules the probe beam propagates through the photo-induced heated region of the sample, experiencing refractive index variations caused by the thermal wave. Each output beam at each mirror is collected by a coupler and sent to separate photodiodes. The backward traveling beam (reflectance) is collected by the same coupler which is used to couple the beam into the cavity. This beam is separated from the forward traveling light coming from the laser source via an optical circulator. The transmitted part is collected by another coupler. In order to transduce a photothermal signal the probe laser frequency is tuned to one side of the interferometer's resonance, i.e. to partial transmission and partial reflectance, respectively. The reflected and transmitted probe beams carry the photothermal signal with apposed sign, but identical intensity noise (see Fig. 1). The signals of the two photodiodes are subtracted by a differential amplifier, enabling the detection of an enhanced photothermal signal with an improved noise figure by cancellation of intensity noise present in both branches.

The primary benefit of the proposed single-cavity balanced-detection ICAPS (single-BICAPS) method is addressed to the reduced number of only one cavity used for noise reduction, compared to the method of balanced-detection ICAPS shown in [19] and [20] using two identical cavities. The use of a single cavity is a main benefit, due to a reduced overall system complexity concerning components and controls.

The method allows for easy adjustment of a high performing balance when locking the probe laser frequency to the cavity's operation point. Efficient noise cancellation requires exactly the same intensity levels of the two probe laser beams at the photodetectors. Any imbalance within the two channels causes a decreased noise cancellation performance or even complete failure of noise reduction. When locking the probe laser frequency to the operation point the reflectance and transmittance channel will respond identically to any drift not requiring an active control of the used cavity. This is not the case for the conventional balanced-detection ICAPS system [19,20]. Here, identical intensities may be difficult to achieve due to individual drifts of the transmission frequencies of the separate cavities e.g. by temperature, typically requiring active control of at least one of the two cavities to compensate any drift and to keep the detected intensities of the two channels as similar as possible.

Within the proposed method the photothermal signal is detected in both, the transmitted and reflected channel. Therefore, the differential amplified output will yield an increased transduced PTS signal by a factor of 2 (6 dB) compared to the conventional balanced-detection ICAPS scheme [19,20], where the photothermal signal is only present

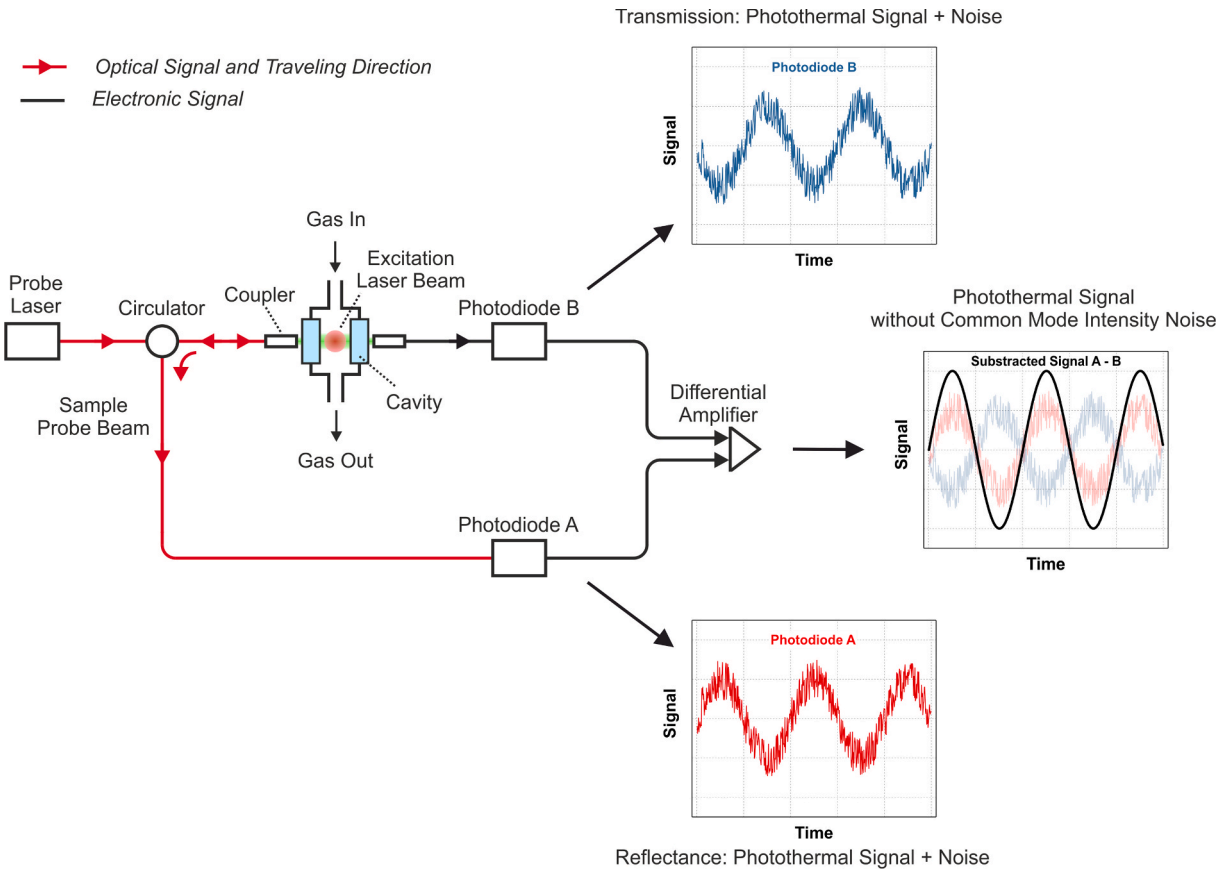

Fig. 1. Principle of balanced-detection ICAPS employing a single cavity. A probe laser is coupled into the cavity of a Fabry-Perot interferometer monitoring the reflected and transmitted beams via individual photodiodes. In case of photothermal excitation both beams carry the photothermal signal with opposed sign and noise. By subtraction of the two photodiode signals, the photothermal signal is received along with an enhancement factor of up to 2 compared to the single trace as well as effective rejection of common mode intensity noise.

in one path.

The proposed single-cavity balanced-detection ICAPS scheme is capable of rejection of the probe laser's intensity noise in principle down to the fundamental limit of shot noise, yielding an improved noise level compared to the basic ICAPS setup not using any balanced-detection scheme [18]. However, probe laser frequency and environmental noise, such as acoustic waves, will not be cancelled but instead will be enhanced by a factor of 2 (6 dB) in the similar way as the photothermal signal. This characteristic of the single-cavity balanced-detection ICAPS scheme is disadvantageous compared to the previous published balanced detection scheme, employing two interferometers [20]. This can be explained by the fact that when performing balanced-detection using two cavities both noise sources, laser frequency and also environmental (acoustic) noise can be efficiently corrected for. For reducing the influence of external acoustic noise in the single-cavity balanced approach implementation of a dedicated acoustic shielding unit, i.e., a proper housing is required. Such an installation, while technically feasible, was not the topic of this study. Probe laser frequency noise, however, can be minimized by using an adequate laser source and driver.

4. Sensor architecture

The architecture of the single-cavity balanced-detection ICAPS based gas sensor employing a fiber-coupled probe laser configuration is depicted in Fig. 2. This setup used a single air-spaced optical cavity, consisting of two fused silica plates ($10 \times 5 \times 2$ mm) on which dielectric-coated mirrors with a reflectivity of $R = 0.989$ were deposited. The mirrors were separated by spacers of 1 mm thickness. The cavity was simultaneously used as the transducer for monitoring induced changes in the refractive index, as well as the reference to apply balanced detection. Photothermal-induced refractive index changes inside the cavity were monitored via a fiber-coupled, single-mode tunable continuous wave (CW), distributed feedback (DFB), fiber laser (FL), acting as the probe laser. This probe laser emitted a beam at a central wavelength of ~ 1550 nm and could be thermally tuned within a total

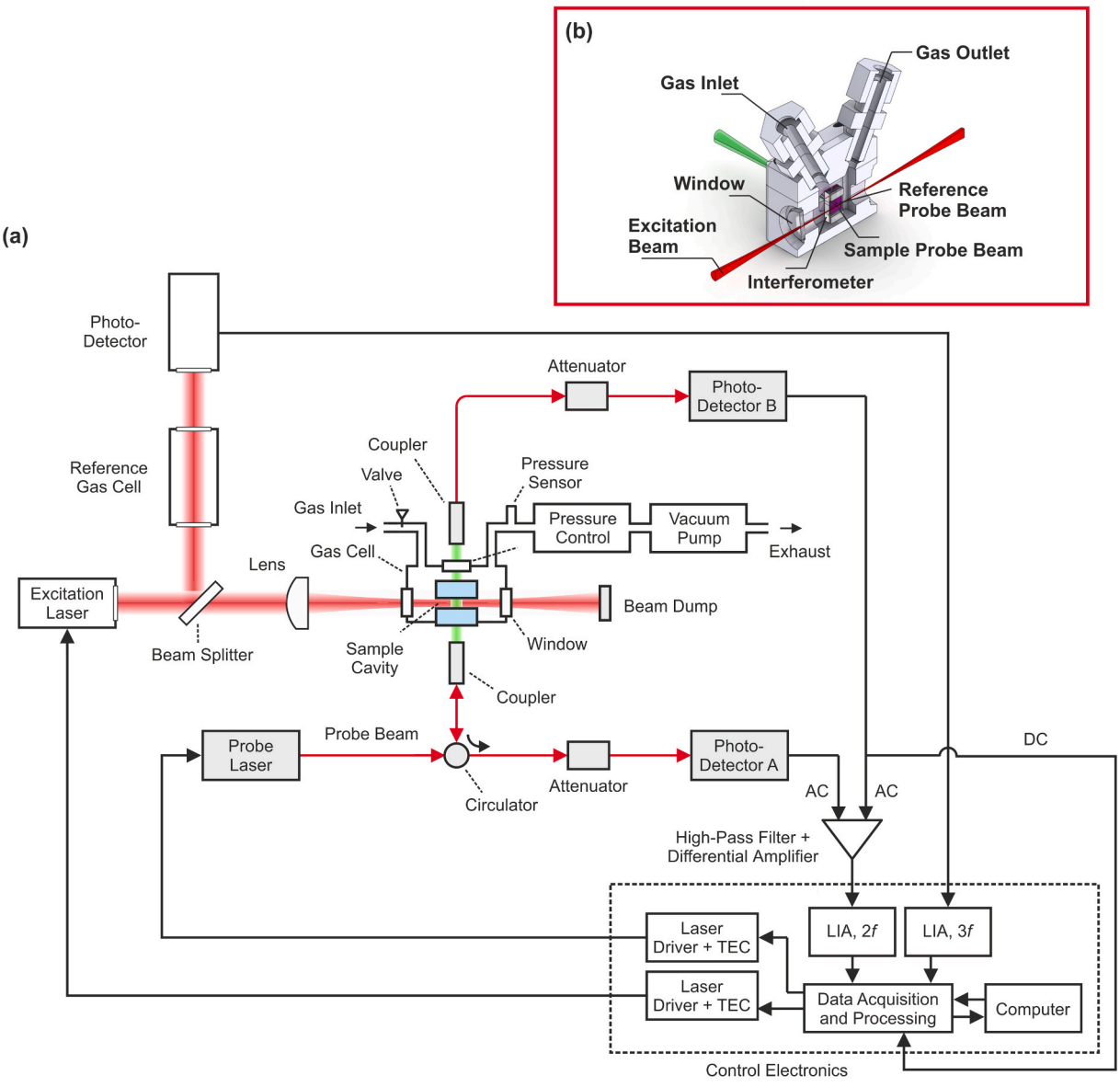

Fig. 2. (a) Schematic of the balanced-detection ICAPS based gas sensor employing a single cavity and a fiber-coupled probe laser configuration, simultaneously monitoring the reflectance and transmission of the Fabry-Perot interferometer; (b) Illustration (section view) of the employed gas cell [28], having a total sample volume of 1.8 cm^3.

range of ~ 1.2 nm. The FL emitted a constant optical output power of 40 mW over its whole tuning range. The fiber-coupled output beam of the probe laser was routed through a fiber-coupled optical circulator whose corresponding port was connected to a fiber-coupled gradient-index (GRIN) collimator. This collimator served to couple the forward traveling light into the cavity and the reflected, backward travelling light again into the fiber. To achieve stable long-term coupling of the probe beam into the interferometer, the fiber-optic collimator was mounted in a robust opto-mechanical GRIN-lens holder. The reflected light was separated from the forward traveling light by the circulator and sent to a photodetector (photodetector A). The transmitted beam was coupled by a further coupler into an optical fiber and again sent to a photodetector (photodetector B). Both detectors consisted of a gallium indium arsenide (GaInAs) positive intrinsic negative junction (PIN) photodiode amplifying the signal via a *trans*-impedance amplifier (TIA). The power of these individually reflected and transmitted beams were adjusted by fiber-coupled attenuators ahead of the detectors to avoid saturation. At the sensor's operation point the power of the reflected and transmitted beam was identical. This yielded the same response to intensity noise in both channels. The electronic outputs of the photodiodes were passed to a 4th order Gaussian high-pass filter with a 3 dB cut-off frequency of 200 Hz and a low-noise differential amplifier with a gain of 100, whose output was fed into a lock-in amplifier (LIA). The probe laser's emission frequency was maintained at the operation point of the cavities' resonance via a slow feedback circuit (mHz), by using the DC component of the photodetector, which monitored the transmitted probe laser intensity (photodetector B). By monitoring the DC-component and adjusting the probe laser frequency, any drift of the transducer, e.g., due to temperature, pressure or changing sample gas composition, or due to a drift of the emitted laser frequency was automatically compensated. The setup used the same gas cell as described in [28], see Fig. 2 (b). The interferometer was fixed on one side into the compact and gas-tight aluminum cell, having a total sample volume of ~ 1.8 cm^3. Transmission of the probe laser beam was enabled by the interferometer substrates and a fused silica window, respectively, transmission of the excitation laser beam through the cell was enabled by two CaF_2 windows. Sample gas exchange was performed via gas in- and outlets. For probing the analyte present in the sample gas inside the interferometer a collimated, high heat load (HHL) packaged CW-DFB quantum cascade laser (QCL) emitting at a wavelength of 4.59 μm (excitation laser) was used, whose frequency could be tuned by varying the QCL temperature via the applied injection current and by temperature control by means of a Peltier element included in the laser mount. The QCL output beam was focused by a plano-convex CaF_2 lens ($f = 50$ mm) between the two mirrors forming the cavity to induce strong photothermal excitation via the high laser intensity, intersecting the standing wave of the probe beam in the transverse direction. The sensor platform was based on photothermal sample excitation via wavelength modulation (WM) and detection of the second harmonic ($2f$) [31] by demodulation of the alternating current (AC) component of the differentially amplified photodetector signals, i.e., the balanced signal, using a lock-in amplifier (LIA). The digitized electronic signals were transferred to a computer for further data processing in a LabVIEW-based program. Additionally, the QCL output beam was split by a beam splitter (97:3), whose low power part was guided through a reference cell filled with CO in N_2 at reduced pressure, and finally onto a pyroelectric photodetector. The reference gas cell and the photodetector were used as the reference channel to monitor the emitted QCL wavelength feeding the detector signal to another LIA. The ICAPS detection was performed in scan mode, where spectra of the sample gas were acquired by slowly tuning (mHz) the QCL frequency over the desired spectral range around the target absorption line through a change of the DC injection current component using a sawtooth function. To implement the WM technique, the emission wavelength of the QCL was modulated by adding a sinusoidal function to the DC injection current input. The pressure and flow of the sample gas inside the measurement cell were controlled and maintained by using a metering valve, pressure sensor, pressure controller, and mini diaphragm vacuum pump. In a previous study [20] it has been shown that an optimum sensor response of an ICAPS system employing comparable components can be found at modulation frequencies around a few 100 Hz showing the highest signal-to-noise ratio at $f_{mod} = 150$ Hz with its corresponding $2f$ detection frequency of 300 Hz. This finding corresponds to the inverse nature of the photothermal signal strength with modulation frequency and the limitation at comparatively low frequencies by electronic $1/f$ noise. In order to be able to facilitate direct comparison to previous publications the metrological figures of merit for the presented sensor were investigated by employing a modulation frequency of $f_{mod} = 297$ Hz, a modulation depth of $\Delta\nu = \pm 0.09$ cm^{-1}, an LIA time constant set to $\tau = 1$ s, and a sawtooth excitation laser tuning frequency of $f = 6.67$ mHz. The absolute pressure and flow of the sample gas was kept constant at $p = 850$ mbar and $u = 25$ mL min^{-1}.

The spacing of the cavity mirrors was chosen to be 1 mm because of several characteristics: The free spectral range (FSR) of a 1-mm spaced cavity is about 150 GHz, which corresponds to a wavelength span of 1.2 nm at the probe laser's central wavelength of 1550 nm. The FSR is same as the total tuning range of the probe laser, being a perquisite to be able to tune its wavelength at least to one inflection point on one side of the cavity's transmission for every potential refractive index of the gas which varies with sample temperature, pressure and composition. A small spacing is advantageous for coupling the probe beam into the cavity achieving high transmission. At the same the slope around the operation point of the cavity's transmission decreases with decreasing spacing, weakening the transduction to photothermal induced signals. Moreover, the generated photothermal wave is highly damped and only expands in the very vicinity of its generation. Therefore, a mirror spacing of 1 mm allows for reasonable well probe laser coupling to the cavity, but also allows for reasonable well transduction of the induced photo-thermal wave. Moreover, a cavity spacing of 1 mm admits for simple transmission of the focused excitation laser beam in the transverse direction without touching any cavity mirrors, which could potentially introduce noise. For this various reasons, a 1-mm cavity mirrors spacing is the sweet spot for achieving sensitive and robust ICAPS measurements.

5. Results

5.1. Overview

In order to verify the functional principle of the proposed sensing scheme, it's metrological figures of merit were determined using carbon monoxide (CO) as target molecule. Investigations of the sensor's noise cancellation and signal enhancement performance were conducted. Also, the influence of water vapor on the photothermal signal was studied, as well as the sensor's sensitivity and linear response were analyzed. Different trace gas concentration levels were obtained by blending a 100 ppmv CO calibration mixture with N_2 via a custom gas mixing system. The N_2 used for dilution could be moisturized with water vapor in a wide concentration range. Spectra of CO were acquired via tuning the QCL frequency across the selected absorption line.

5.2. Signal enhancement and noise reduction

In order to confirm the enhancement of the detected photothermal signal of the presented setup two spectra of 10 ppmv CO in N_2 were acquired (see Fig. 3): the first spectrum was recorded when balanced detection was deactivated, i.e. only the signal of photodiode A was recorded (see Fig. 3 red trace, non balanced-detection). Next a spectrum in active balanced detection mode was recorded (see Fig. 3, blue trace, balanced detection). Comparison of the two spectra shows an improvement in the detected signal amplitude by a factor of approximately 1.9 when employing balanced-detection. This result is in very

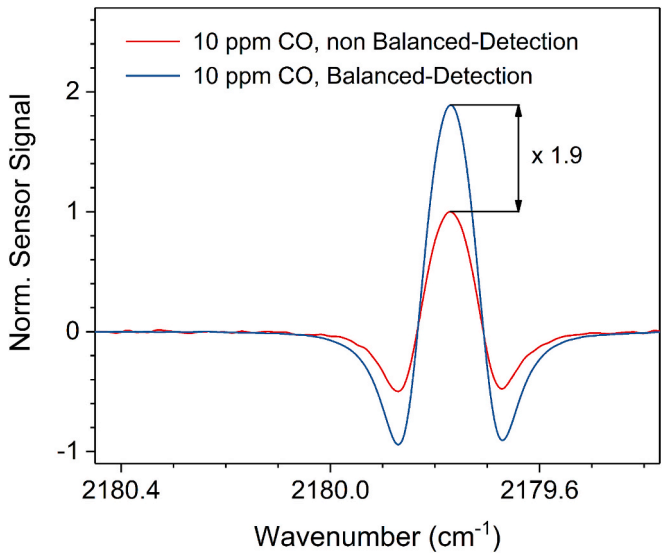

Fig. 3. Normalized 2f-WM single-cavity ICAPS sensor response for non balanced-detection (red trace) and balanced-detection (blue trace) operation, when the QCL frequency was tuned across the targeted CO absorption band centered at 2179.77 cm^{-1} at an absolute pressure of 850 mbar.

good agreement with the maximum achievable value of 6 dB (factor 2). The small deviation of the measured data from the maximum theoretical enhancement factor may have been caused by a small experimental discrepancy in the absolute power levels at the photodetectors caused by a small mismatch of the transmission's and reflectance's resonance height, causing a slightly different transduction to the photothermal signal in the two channels.

To investigate the noise cancellation performance of the presented configuration, the noise floor of the sensor was recorded again for both settings, the non balanced-detection and the balanced detection mode. Each setting was recorded for a total duration of 30 min when the cell was flushed with moisturized N_2 and the QCL frequency was kept at 2179.77 cm^{-1}. The results of the two measurements are shown Fig. 4. Comparison of the calculated standard deviations of the measured data show a noise reduction by a factor of approximately 9.7, when employing the balanced-detection scheme.

In total, the measured results show an improvement in the sensor's signal-to-noise ratio by a factor of ~ 18, when employing balanced detection compared to non-balanced operation. The improvement in the signal-to-noise ratio is composed one the one hand by an enhancement of the signal by a factor of 1.9, and on the other hand by a reduction in noise by a factor of 9.7. This result clearly highlights the benefit of the single-cavity balanced-detection ICAPS operation mode.

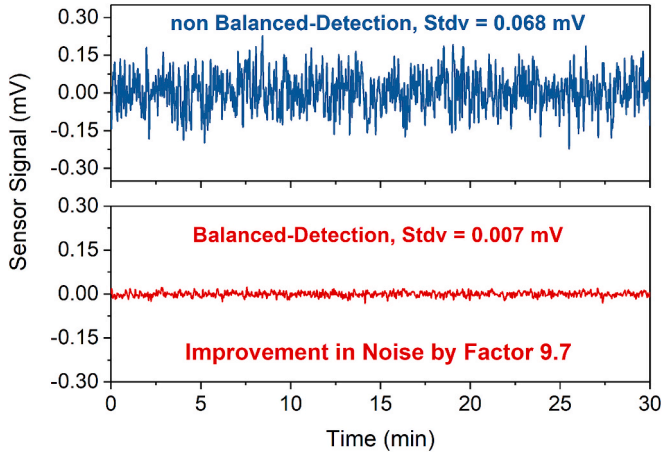

Fig. 4. 2f-WM ICAPS sensor response for non balanced detection (blue trace) and balanced detection within a single cavity (red trace) for pure N_2 when the QCL was kept at 2179.77 cm^{-1} at an absolute sample pressure of 850 mbar.

5.3. *Influence of water vapor on the CO ICAPS signal*

In order to investigate the influence of varying water vapor concentration on the detected photothermal CO signal of the presented ICAPS based sensor, two different experiments are reported:

First, the sensor signal for 10 ppm CO as a function of the H_2O concentration was recorded. The dependence of the signal amplitudes versus absolute humidity is shown in Fig. 5. The results show an initial decrease of the recorded photothermal signal with increasing humidity reaching a minimum at 0.18 vol% H_2O, before increasing with increasing humidity. A maximum improvement of the measured ICAPS signal by a factor of approximately 7.7 was received, when the analyzed gas mixture was humidified with 2.1 vol% H_2O. This behavior can be explained by competing endothermal and exothermal pathways of the vibrational relaxation of CO in N_2 and H_2O, and is discussed in detail in [32].

Second, a spectra of 10 ppmv CO in dry N_2 and humidified N_2 were acquired, see Fig. 6. The result again proofs the photothermal signal enhancement via molecular V-T relaxation by a factor of 7.7 when the analyzed sample has a water content of 2.1 vol%, clearly showing no spectroscopic interference with water within the analyzed spectral region.

In practical applications the analyte often needs to be quantified in gas mixtures with unknown water content, potentially varying in a range from 0 to 100 % relative humidity. To correct for the dependence of the system's CO signal amplitude on the water content, the humidity of the sample gas has to be measured additionally. With the measured information on the water concertation the CO signal strength can be corrected by software according to the characterized dependency shown in Fig. 5. The H_2O concentration of the sample gas can be measured simply using an additional humidity and temperature sensor, e.g. the sensor which was used in this work (SHT85, Sensirion AG). Alternatively, the water content could be measured spectroscopically by the ICAPS system itself using an H_2O absorption band which is in the tuning range of the employed QCL. For the presented system the water band centered at 2181.33 cm^{-1} could be used, which is neighboring the CO absorption band centered at 2179.77 cm^{-1}. However, this approach is

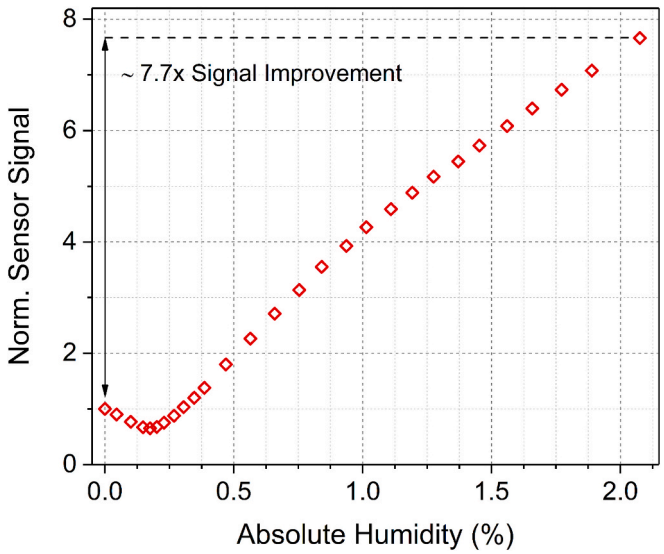

Fig. 5. Dependence of the 2f-WM ICAPS signal amplitudes on the H_2O concentration (c_{CO} = 10 ppm, p = 850 mbar, $\Delta\nu = \pm 0.09$ cm^{-1}).

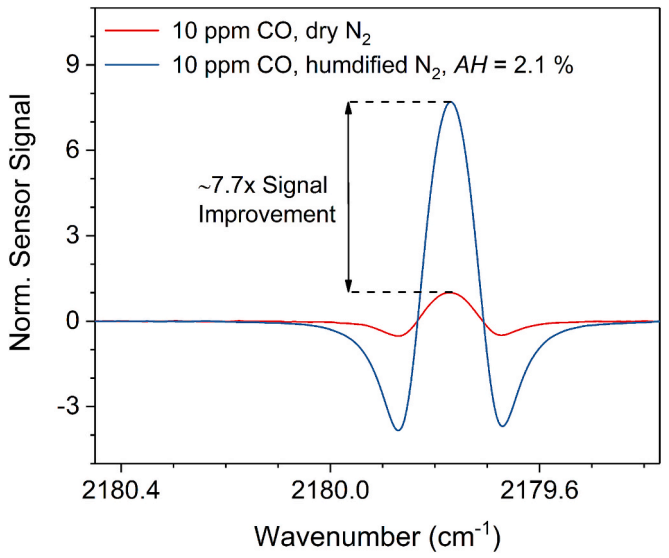

Fig. 6. 2f-WM ICAPS signals for 10 ppmv CO in dry and moisturized N_2, when the QCL was tuned across the absorption line located at 2179.99 cm^{-1} (p = 850 mbar, m = ±0.09 cm^{-1}).

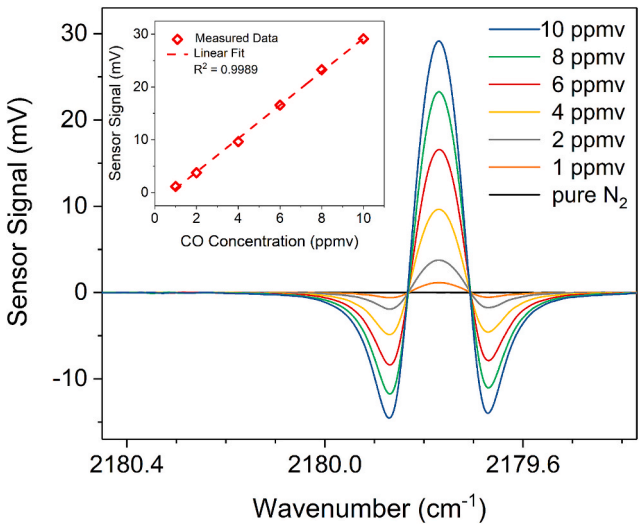

Fig. 7. 2f-WM single-cavity balanced-detection ICAPS sensor response for six different CO gas concentrations in moisturized N_2 (c_{H2O} = 2.1 vol%) as well as the sensor noise floor for moisturized N_2, recorded when the QCL frequency was tuned over the targeted absorption band centered at 2179.77 cm^{-1} at an absolute pressure of 850 mbar. (b) Measured signal amplitudes as a function of CO concentration.

more time consuming as two individual absorption lines have to be probed alternately.

Moreover, the sample gas could be humidified before analysis to establish consistent humidification. This approach is often used in quartz-enhanced photoacoustic spectroscopy (QEPAS) setups whose sensor signals are commonly also dependent on the sample's water concertation due to additional molecular V-T relaxation pathways of the analyte [15,33]. If the sample is humidified to nearby 100 % relative humidity before analysis, the sensor's sensitivity will be highest and at optimum working conditions due to maximum enhancement of the V-T relaxation. This approach can be realized by using e.g. a polydimethylsiloxane membrane for humidifying the sample gas. However, this approach entails disadvantages like increased need of sample gas volume, different membrane permeability coefficients of various gases and additional maintenance requirements.

5.4. Sensitivity and linear response of the sensor

The selective response of the single-cavity balanced-detection ICAPS sensor to various concentrations of CO in moisturized N_2 was analyzed by recording 2*f*-WM spectra for six different trace gas levels in the range from 1 to 10 ppmv, together with the noise floor of the sensor for moisturized N_2 (see Fig. 7). Based on the signal amplitude for 10 ppmv CO and the standard deviation of the noise level for moisturized N_2, a signal-to-noise ratio of ~ 4103 was calculated, which yields a 1σ minimum detection limit (MDL) of ~ 2 ppbv for an acquisition time of 1 s. The normalized noise equivalent absorption (NNEA) coefficient at unit laser power and bandwidth was calculated to be NNEA = 7.4×10^{-9} cm^{-1} W $Hz^{-1/2}$, using a minimum detectable CO absorption coefficient of $\alpha_{min} = 6.51 \times 10^{-8}$ cm^{-1}, an optical excitation power of $P = 35$ mW, and an LIA detector bandwidth of $\Delta f = 94$ mHz ($\tau = 1$ s, 18 dB/oct low-pass filter). Moreover, the sensor yielded excellent linearity between the measured signal amplitudes and the CO concentration (see inset, Fig. 7).

5.5. Long-term stability

To analyze the noise characteristics and long-term stability of the single-cavity balanced-detection ICAPS setup, an Allan-Werle deviation investigation [31] was performed. Data were recorded for an overall time period of 8 h in the controlled conditions of the laboratory employing the LIA settings described above, i.e., a detection bandwidth of $\Delta f = 0.094$ Hz with an 18 dB/oct low-pass filter. During the measurement the cell was flushed with pure N_2. The Allan-Werle plot of the measurement is depicted in Fig. 8. The plotted Allan-Werle deviation indicates excellent long-term stability of the sensor, showing that the single-cavity balanced-detection ICAPS system is dominated by white noise characteristics, as any additional sensor drift is inherently compensated by the probe laser lock described in Section 4. If required, this white-noise dominated region allows for signal averaging up to a few thousands of seconds, proportionally improving the sensor's sensitivity.

6. Conclusions

The presented work demonstrates sensitive and compact trace gas detection by the implementation of a new balanced-detection scheme to the ICAPS configuration, employing only a single cavity. This layout was realized by the simultaneous monitoring of the cavity's transmission and

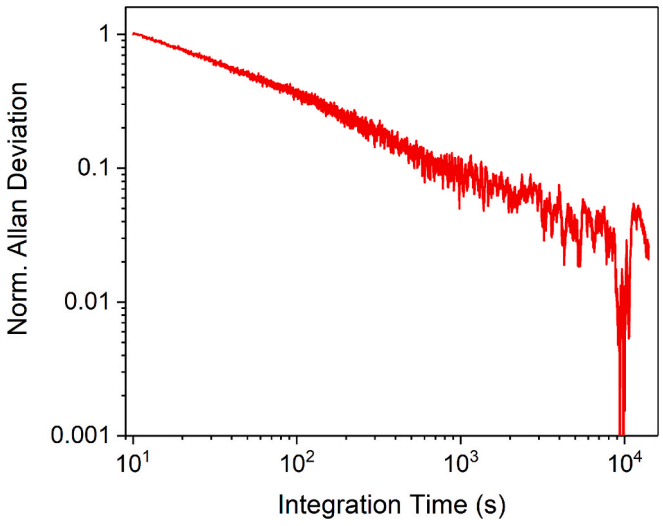

Fig. 8. Allan-Werle deviation plot of the sensor noise recorded over a time period of 8 h.

reflection, utilizing a fiber-coupled probe laser configuration. The capabilities of the method were demonstrated on the example of CO detection, exploiting a CW-DFB-QCL as the excitation source to target strong fundamental absorption features of the sample molecules in the mid-infrared region. The single-cavity balancing method demonstrated substantial advancement in the analytical figures of merit compared to the basic ICAPS scheme [18] by cancellation of common mode noise present in both detection branches and by an enhancement of the detected photothermal signal, resulting in a total improvement of the signal-to-noise ratio by a factor of 18. The 1σ MDL was determined to be 2 ppbv CO in moisturized N_2, employing a 1 s integration time. This value corresponds to NNEA of 7.4×10^{-9} cm^{-1} W Hz$^{-1/2}$. In this work also the influence of water vapor on the photothermal signal through its role in the V-T relaxation process of CO has been investigated in detail. For practical applications the photothermal cross-sensitivity to water has to be considered. Strategies for compensating this influence have been discussed, such as independent moisture sensing and software correction. The presented layout offers a simple beam alignment, enabling a robust and compact gas sensor design. High sensitivity was accomplished by application of interferometers with moderate finesse as well as a small mirror spacing of 1 mm together with strong photothermal signal generation by use of high excitation laser intensities. Additionally, the system showed excellent long-term stability due to feedback-controlled compensation of any transducer drifts. This characteristic potentially allows to improve sensitivity by application of long-term integration times. The presented sensor is based on a compact arrangement with a total cell volume of only 1.8 ml, and shows high potential for further miniaturization, even down to photonic integration on a chip. Since the ICAPS technique is based on indirect detection, this method is not limited to a particular excitation wavelength range but can be applied to a broad range of excitation sources. Also, more than one excitation source may be coupled to the transducer, allowing for multi-component analysis. Additionally, the robust transducer element holds potential for use in elevated temperature and pressure applications. In conclusion, the method of single-cavity balanced-detection ICAPS offers a substantial improvement in the sensor's sensitivity compared to the basic ICAPS configuration [18], when operated under conditions without additional probe laser frequency and environmental noise contribution. Moreover, the method features an alternative noise cancellation method with less system complexity and simplified control of signal balancing, compared to the powerful balanced-detection ICAPS scheme employing two cavities [20].

CRediT authorship contribution statement

Johannes P. Waclawek: Writing – review & editing, Writing – original draft, Visualization, Software, Methodology, Investigation, Data curation, Conceptualization. **Harald Moser:** Writing – review & editing, Software, Data curation. **Ufuk Yilmaz:** Data curation. **Bernhard Lendl:** Writing – review & editing, Resources.

Declaration of competing interest

The authors declare that they have no known competing financial interests or personal relationships that could have appeared to influence the work reported in this paper.

Acknowledgement

Funding was provided by the European Union's Horizon Europe research and innovation programme through the BROMEDIR research project under grant agreement No. 101092697 and the M3NIR research project under grant agreement No. 101093008.

Data availability

Data will be made available on request.

References

[1] H. Moser, W. Pölz, J.P. Waclawek, J. Ofner, B. Lendl, Implementation of a quantum cascade laser-based gas sensor prototype for sub ppmv H_2S measurements in a petrochemical process gas stream, Anal. Bioanal. Chem. 409 (2016) 729–739.
[2] D. Yun, R. Cole, N. Malarich, S. Coburn, N. Hoghooghi, J. Liu, J. France, M. Hagenmaier, K. Rice, J. Donbar, G. Rieker, Spatially resolved mass flux measurements with dual-comb spectroscopy, Optica 9 (2022) 1050–1105.
[3] M.G. Soskind, N.P. Li, D.P. Moore, Y. Chen, L.P. Wendt, J. McSpiritt, M.A. Zondlo, G. Wysocki, Stationary and drone-assisted methane plume localization with dispersion spectroscopy, Remote Sens. Environ. 289 (2023).
[4] J.B. McManus, M.S. Zahniser, D.D. Nelson, J.H. Shorter, S.C. Herndon, D. Jervis, M. Agnese, R. McGovern, T.I. Yacovitch, J.R. Roscioli, Recent progress in laser-based trace gas instruments: Performance and noise analysis, Appl. Phys. B 119 (2015) 203–218.
[5] K. Owen, A. Farooq, A calibration-free ammonia breath sensor using a quantum cascade laser with WMS 2f/1f, Appl. Phys. B 116 (2013) 371–383.
[6] A. Nataraj, M. Gianella, I. Prokhorov, B. Tuzson, M. Bertrand, J. Mohn, J. Faist, L. Emmenegger, Quantum cascade laser absorption spectrometer with a low temperature multipass cell for precision clumped CO2 measurement, Opt. Express 30 (2022) 4631.
[7] M. Graf, P. Scheidegger, A. Kupferschmid, H. Looser, T. Peter, R. Dirksen, L. Emmenegger, B. Tuzson, Compact and lightweight mid-infrared laser spectrometer for balloon-borne water vapor measurements in the UTLS, Atmos. Meas. Tech. 14 (2021) 1365–1378.
[8] A. Klein, O. Witzel, V. Ebert, Rapid, time-division multiplexed, direct absorption- and wavelength modulation-spectroscopy, Sensors 14 (2014) 21497–21513.
[9] C.S. Goldenstein, C.L. Strand, I.A. Schultz, K. Sun, J.B. Jeffries, R.K. Hanson, Fitting of calibration-free scanned-wavelength-modulation spectroscopy spectra for determination of gas properties and absorption lineshapes, Appl. Opt. 53 (2014) 356–367.
[10] P. Kluczynski, J. Gustafsson, Å.M. Lindberg, O. Axner, Wavelength modulation absorption spectrometry - an extensive scrutiny of the generation of signals, Spectrochim. Acta Part b: Atom. Spectrosc. 56 (8) (2001) 1277–1354.
[11] J. Li, H. Deng, J. Sun, B. Yu, H. Fischer, Simultaneous atmospheric CO, N2O and H2O detection using a single quantum cascade laser sensor based on dual-spectroscopy techniques, Sens. Actuators B 231 (2016) 723–732.
[12] N. Liu, L. Xu, S. Zhou, L. Zhang, J. Li, Simultaneous detection of multiple atmospheric components using an NIR and MIR laser hybrid gas sensing system, ACS Sensors 5 (11) (2020) 3607–3616.
[13] R.F. Curl, F. Capasso, C. Gmachl, A.A. Kosterev, J.B. McManus, R. Lewicki, M. Pusharsky, G. Wysocki, F.K. Tittel, Quantum cascade lasers in chemical physics, ChemPhy. Lett. 487 (2010) (2010) 1–18.
[14] Q. Huang, Y. Wei, J. Li, Simultaneous detection of multiple gases using multi-resonance photoacoustic spectroscopy, Sens. Actuators B 369 (2022) 132234.
[15] A. Zifarelli, R. De Palo, P. Patimisco, M. Giglio, A. Sampaolo, S. Blaser, J. Butet, O. Landry, A. Müller, V. Spagnolo, Multi-gas quartz-enhanced photoacoustic sensor for environmental monitoring exploiting a Vernier effect-based quantum cascade laser, Photoacoustics 28 (2022) 100401.
[16] S.E. Bialkowski, N.G.C. Astrath, M.A. Proskurnin, Photothermal Spectroscopy Methods, second edition, John Wiley & Sons, 2019.
[17] A.J. Campillo, S.J. Petuchowski, C.C. Davis, H.-B. Lin, Fabry-Perot photothermal trace detection, Appl. Phys. Lett. 41 (4) (1982) 327–329.
[18] J.P. Waclawek, V.C. Bauer, H. Moser, B. Lendl, 2f-wavelength modulation Fabry-Perot photothermal interferometry, Opt. Express 24 (2016) 28958–28967.
[19] J.P. Waclawek, C. Kristament, H. Moser, B. Lendl, Balanced-detection interferometric cavity-assisted photothermal spectroscopy, Opt. Express 9 (2019) 12183–12195.
[20] J.P. Waclawek, H. Moser, B. Lendl, Balanced-detection interferometric cavity-assisted photothermal spectroscopy employing an all-fiber-coupled probe laser configuration, Opt. Express 5 (2021) 7794–7808.
[21] D. Pinto, H. Moser, J.P. Waclawek, S.D. Russo, P. Patimisco, V. Spagnolo, B. Lendl, Parts-per-billion detection of carbon monoxide: a comparison between quartz-enhanced photoacoustic and photothermal spectroscopy, Photoacoustics 22 (2021).
[22] P. Breitegger, B. Lang, A. Bergmann, Intensity Modulated Photothermal Measurements of NO_2 with a Compact Fiber-coupled Fabry–Pérot Interferometer, Sensors 19 (2019) 3341.
[23] F. Yang, Y. Tan, W. Jin, Y. Lin, Y. Qi, H.L. Ho, "Hollow-core fiber Fabry-Perot photothermal gas sensor, Opt. Lett. 41 (2016) 3025–3028.
[24] W. Jin, Y. Cao, F. Yang, H.L. Ho, Ultra-sensitive all-fibre photothermal spectroscopy with large dynamic range, Nat. Commun. 6 (2015) 6767.
[25] P. Zhao, Y. Zhao, H. Bao, H.L. Ho, W. Jin, S. Fan, S. Gao, Y. Wang, P. Wang, Mode-phase-difference photothermal spectroscopy for gas detection with an anti-resonant hollow-core optical fiber, Nat. Comm. 11 (2020) 847.
[26] Y. Zhao, W. Jin, Y. Lin, F. Yang, H.L. Ho, All-fiber gas sensor with intracavity photothermal spectroscopy, Opt. Lett. 43 (2018) 1566–1569.
[27] K. Krzempek, G. Dudzik, K. Abramski, Photothermal spectroscopy of CO_2 in an intracavity mode-locked fiber laser configuration, Opt. Express 22 (2018) 28861–28871.

[28] G. Malvicini, J.P. Waclawek, D. Pinto, H. Moser, S. Iadanza, K. Gradkowski, L. O'Faolain, B. Lendl, Balanced-detection interferometric cavity-assisted photothermal spectroscopy via collimating fiber-array integration, Sens. Actuators B 412 (2024) 135766.
[29] F.L. Pedrotti, L.M. Pedrotti, L.S. Pedrotti, Introduction to Optics, 3rd, Edition (Cambridge University Press), 2017.
[30] N. Hodgson, H. Weber, Laser Resonators and Beam Propagation, 2nd ed., Springer, 2005. Part II.
[31] P. Werle, A review of recent advantages in semiconductor laser based gas monitors, Spectrochim. Acta A 54 (1998) 197–236.
[32] J. Hayden, B. Baumgartner, B. Lendl, Anomalous humidity dependence in photoacoustic spectroscopy of CO explained by kinetic cooling, Appl. Sci. 10 (2020) 843.
[33] Y. Ma, R. Lewicki, M. Razeghi, F.K. Tittel, QEPAS based ppb-level detection of CO and N2O using a high power CW DFB-QCL, Opt. Express 21 (2013) 1008–1019.